Materials Today Bio 26 (2024) 101047

Contents lists available at ScienceDirect

Materials Today Bio

journal homepage: www.journals.elsevier.com/materials-today-bio

Pt/NiFe-LDH hybrids for quantification and qualification of polyphenols

Chunmeng Ding [a,b,1], Yuexing Zhu [c,1], Zhiyuan Huo [a], Shouzhi Yang [b], Yan Zhou [a], Ayizekeranmu Yiming [b], Wei Chen [b], Shanrong Liu [c,**], Kun Qian [b,***], Lin Huang [a,d,*]

[a] Department of Clinical Laboratory Medicine, Shanghai Chest Hospital, Shanghai Jiao Tong University, Shanghai, 200030, P. R. China
[b] State Key Laboratory of Systems Medicine for Cancer, School of Biomedical Engineering, Institute of Medical Robotics and Shanghai Academy of Experimental Medicine, Shanghai Jiao Tong University, Shanghai, 200030, P. R. China
[c] Second Military Medical University, Changhai Hospital, Department of Lab Diagnostics, Shanghai, 200433, P. R. China
[d] Institute of Thoracic Oncology, Shanghai Chest Hospital, Shanghai Jiao Tong University School of Medicine, Shanghai, 200030, P. R. China

ARTICLE INFO

Keywords:
Polyphenol
Pt/NiFe-LDH hybrid
Nanozyme
Laser desorption/ionization mass spectrometry
Quantification
Qualification

ABSTRACT

Polyphenols with antioxidant properties are of significant interest in medical and pharmaceutical applications. Given the diverse range of activities of polyphenols in vivo, accurate detection of these compounds plays a crucial role in nutritional surveillance and pharmaceutical development. Yet, the efficient quantitation of polyphenol contents and qualification of monomer compositions present a notable challenge when studying polyphenol bioavailability. In this study, platinum-modified nickel-iron layered double hydroxide (Pt/NiFe-LDH hybrids) were designed to mimic peroxidases for colorimetric analysis and act as enhanced matrices for laser desorption/ionization mass spectrometry (LDI MS) to quantify and qualify polyphenols. The hybrids exhibited an enzymatic activity of 33.472 U/mg for colorimetric assays, facilitating the rapid and direct quantitation of total tea polyphenols within approximately 1 min. Additionally, the heterogeneous structure and exposed hydroxyl groups on the hybrid surface contributed to photoelectric enhancement and *in-situ* enrichment of polyphenols in LDI MS. This study introduces an innovative approach to detect polyphenols using advanced materials, potentially inspiring the future development and applications of other photoactive nanomaterials.

1. Introduction

Polyphenols are essential metabolites, acting as the primary endogenous antioxidants of plants [1]. Specifically, tea polyphenols possess antioxidant, anti-inflammatory, anticancer, and lipid metabolism-regulating properties, and have been extensively utilized in disease prevention and treatment. This is attributed to their phenolic hydroxyl structure, enabling the scavenging of free radicals and the regulation of various types of oxidases in the body [2,3]. On one hand, the levels of total polyphenols serve as important indicators of physiological processes, such as estimating the average daily intake of total polyphenols toward nutritional evaluation [4,5]. On the other hand, the facile monitoring of the delivery and metabolism of polyphenol monomers during disease medication is essential for evaluating therapy efficacy [6,7]. Therefore, both the quantification of total polyphenols and the qualification of different polyphenol fingerprints bear significant implications for the bioavailability of polyphenols.

However, the instability of polyphenols (such as tea polyphenol) during storage and drug delivery presents challenges in quantifying and qualifying catechins. For the former, colorimetric analysis enables the quantification of total polyphenols, but faces obstacles in the specific identification and precise monitoring of individual catechin monomers [8]. Moreover, the color change accompanied with redox reaction can be further improved by utilizing nanozymes with enhanced stability compared to natural enzymes (*e.g.*, peroxidase) [9–11]. For the latter, high-performance liquid chromatography is commonly required for the determination of polyphenol monomers, limited for clinical applications due to high sample consumption, complex sample preparation requirements, and time-intensive procedures [12]. In contrast, laser desorption/ionization mass spectrometry (LDI MS) is an essential analytical technique in macromolecular investigation, due to its rapid analysis capabilities within seconds and minimal sample consumption.

* Corresponding author. Department of Clinical Laboratory Medicine, Shanghai Chest Hospital, Shanghai Jiao Tong University, Shanghai, 200030, China.
** Corresponding author.
*** Corresponding author.
E-mail addresses: liushanrong01@126.com (S. Liu), k.qian@sjtu.edu.cn (K. Qian), linhuang@shsmu.edu.cn (L. Huang).
[1] These authors contributed equally to this work and should be considered co-first authors.

https://doi.org/10.1016/j.mtbio.2024.101047
Received 1 February 2024; Received in revised form 27 March 2024; Accepted 2 April 2024
Available online 3 April 2024

In particular, nanomaterial-enhanced LDI MS has been adopted for the molecular identification of small molecules (molecular weight <1000 Da) [13,14]. Nevertheless, the rational design of advanced nanomaterials as matrices decides the interactions between metabolites and substrate materials for efficient desorption/ionization [15,16].

Advanced materials function as efficient incorporated tools to construct an integrated platform, considering their tunable physicochemical properties [17]. To date, noble metal nanomaterials (such as Au, Ag, and Pt) stand out as candidates for improving both colorimetric and LDI MS applications, regarding their localized surface plasmon resonance (LSPR) effects and photo-thermal properties [18,19]. In particular, Pt nanoparticles (NPs) facilitate the movement of interfacial electrons, by reducing the kinetic barrier with a higher metal work function of 5.65 eV (*e.g.*, 5.1 eV for Au and 4.26 eV for Ag) [20,21], showing promise in improving both catalytic activity and ionization efficiency. However, metal NPs are susceptible to self-aggregation and low surface-to-volume ratios. In addition to noble metals, layered double hydroxide (LDH), a class of inorganic layered materials with unique optical and electric properties, is widely used as a carrier substrate for metal NPs [22]. Metal-LDH hybrids displayed elevated catalytic activity with substantial surface area and synergistic effects. Such hybrids have been applied as adsorbents and catalysts in a wide range of applications such as formaldehyde decomposition, oxygen evolution reaction, water splitting, and nitrate adsorption [23–26]. The incorporation of LDH as a support not only diminishes the size of metal NPs but also hinders their agglomeration, enhancing the catalytic effectiveness of metal-LDH hybrids. Benefitting from the high absorption and large surface area, LDH can serve as a carrier material in nanozymes for colorimetric analysis and matrices for LDI MS [22]. Importantly, the abundance of hydroxyl groups on LDH allows for the selective trapping of hydroxyl-containing molecules, such as polyphenols [27]. Hence, the hybrid composites, comprising these two building blocks, hold promise for developing an integrated platform for polyphenol detection, by combining their individual strengths and synergistic effects.

In this study, we developed Pt/NiFe-LDH hybrids to act as peroxidase mimics for colorimetric analysis and enhanced matrices for LDI MS to quantify and qualify polyphenols, respectively. We synthesized the designed host-guest interfaces between Pt and NiFe-LDH sheets using a facile one-pot ultrasound method. Upon optimization, the hybrids displayed an enzymatic activity of 33.472 U/mg for colorimetric assays, enabling direct quantitation of total tea polyphenols at high speed (~1 min). The colorimetric results yielded statistically comparable outcomes with those from a standard method kit (Folin-Ciocalteu colorimetric method). Furthermore, the heterogeneous structure and exposed hydroxyl groups of the hybrids facilitated photoelectric enhancement and *in-situ* enrichment of polyphenols in LDI MS. This study proposed a novel strategy for polyphenol detection using advanced materials, inspiring future development and applications of other photoactive nanomaterials.

2. Experimental section

2.1. Materials

Chloroplatinic acid hexahydrate ($H_2PtCl_6{\cdot}6H_2O$, 37%), ethanol (99.7%), 30% H_2O_2 solution, and sucrose (Suc) were procured from Sinopharm Chemical Reagent Beijing Co., Ltd (China). Methanol (99.8%) and acetonitrile were ordered from Fisher Chemical (USA). Sodium borohydride ($NaBH_4$, 99%) was purchased from Fluka (German). 3,3′,5,5′-Tetramethylbenzidine (TMB), dimethylsulfoxide (DMSO, 99.8%), (−)-epicatechin (EC, 97%), (−)-epigallocatechin (EGC, 98%), (−)-epigallocatechin gallate (EGCG), tea polyphenol (98%), ascorbic acid (AA, 99%), and chlorogenic acid were ordered from Aladdin Reagent Co., Ltd (China). L-alanine (Ala, 98%), L-serine (Ser), L-lysine (Lys, 98%), D-(+)-glucose (Glc, 99.5%), bovine serum albumin (BSA, 98%), α-cyano-4-hydroxycinnamic acid (CHCA, 99%), and 2,5-dihydroxybenzoic acid (DHB) were purchased from Sigma-Aldrich (USA). Theanine and NaAc-HAc buffer (0.2 M, pH 3.7) was purchased from Shanghai Yuanye Bio-Technology Co., Ltd (China). Arabinose was purchased from Shanghai Titan Scientific Co., Ltd, (China). Rhamnose was ordered from Meryer (Shanghai) Chemical Technology Co., Ltd. (China). (−)-epicatechin gallate (ECG, 98%) was purchased from Baoji Herbest Bio-Tech Co., Ltd (China). Sodium chloride (NaCl) was purchased from Tianjin Chemical Reagent Research Institute Co., Ltd (China). NiFe layered double hydroxide (NiFe-LDH) and gold nanoparticles (Au NPs) were acquired from Jiangsu XFNANO Materials Technology Co., Ltd. (China). Ferulic acid, nickel nanoparticles (Ni NPs), and iron nanoparticles (Fe NPs) were ordered from Shanghai Macklin Biochemical Technology Co., Ltd (China).

2.2. Preparation of Pt/NiFe-LDH hybrids

Synthesis of Pt/NiFe-LDH hybrids followed an ultrasound-assisted reduction method [28]. 50 mg of NiFe-LDHs were dispersed in 100 mL of deionized water (DIW) by ultrasonication (360 W) for 30 min. 50 mL of chloroplatinic acid solution (10 mM) was added into NiFe-LDH solution and then ultrasonicated for 10 min. Then, 50 mL of fresh sodium borohydride solution in an ice bath was slowly added to the mixture and ultrasonicated for 30 min. The blackish turbid solution was obtained and centrifuged at 10000 rpm for 5 min. The precipitates were washed four times with ethanol and DIW, and then dried at 60 °C to obtain Pt/NiFe-LDH hybrids as the final product. The hybrids were optimized through variation of the volume of chloroplatinic acid solution (10 mM; 10 mL, 25 mL, 75 mL, and 100 mL), following the same synthesis approach. Pt NPs were synthesized using the same method in Pt/NiFe-LDH hybrid synthesis.

2.3. Characterization of Pt/NiFe-LDH hybrids

Scanning electron microscope (SEM) and selected area electron diffraction (SAED) were conducted to analyze the morphological and crystallographic characteristics using Gremini 300 (ZEISS, Germany). The distribution and abundance of platinum nanoparticles (Pt NPs) on the Pt/NiFe-LDH hybrids were quantified using transmission electron microscopy (TEM) and energy-dispersive X-ray spectroscopy (EDS) using FEI Talos F200s (Thermo Fisher Scientific Inc., USA). X-ray powder diffraction (XRD) pattern was acquired utilizing a D8 ADVANCE diffractometer (Bruker, USA). The measurements were conducted at 60 kV and 80 mA utilizing copper K-alpha emission and a ceramic X-ray tube. Ultraviolet–visible (UV–vis) spectra between 200 and 800 nm were collected using UV1900 (Shimadzu Ltd., Tokyo, Japan). The X-ray photoelectron spectroscopy (XPS) was recorded on a powder sample using ESCALAB 250xi (Thermo Fisher Scientific Inc., USA) with Al Kα radiation.

2.4. Catalytic activity of Pt/NiFe-LDH hybrids

Peroxidase activity of Pt/NiFe-LDH hybrids was quantified following a standardization method [29]. The reaction was performed through the amalgamation of 50 μL of 3,3′,5,5′-tetramethylbenzidine (TMB) solution (10 mg/mL in DMSO) with 1 mL of NaAc-HAc buffer (0.2 M, pH 3.7) and different quantities of Pt/NiFe-LDH (0.6, 0.7, 0.8, 0.9, and 1.0 μg). Then, 116.8 μL 30% H_2O_2 solution was added to the mixtures. The absorbance value of the mixtures at the wavelength maximum (λ_{max}) of 652 nm was immediately recorded by a microplate reader (SpectraMax i3x, Austria) every 10 s for a total of 1 min. The catalytic activity was determined using the following equation:

$$b_{nanozyme} = V/(\varepsilon \times l) \times (\triangle A/\triangle t) \quad (1)$$

$$SA = b_{nanozyme}/m \quad (2)$$

where $b_{nanozyme}$ referred to the catalytic activity of nanozyme; the total

volume of the reaction solution was denoted as V; ε was the molar absorption coefficient as 39,000/(M cm) for TMB at 652 nm; the length traversed by the light within the microplate was denoted as l; the initial rate of change of light absorbance per minute was expressed as $\triangle A/\triangle t$; SA represented the activity units per milligram of nanozyme; and m signified the weight of nanozymes. The stability of nanozymes was evaluated under different pH (3.5–5.5), temperature (25–65 °C), and storage time (0–15 days).

For the quantitation of tea polyphenol, 1 μL Pt/NiFe-LDH-50 hybrids (1 mg/mL) and 50 μL of TMB (1 mM) were added in 1 mL HAc-NaAc buffer. Then, 50 μL standard tea polyphenols solution was added to the peroxidase-like system. 25 μL H_2O_2 was mixed with the above system and the absorbance at λ_{max} of 652 nm was recorded at 1 min. 3 kinds of tea beverages (green, black, and oolong tea) were diluted 20 times for determination.

2.5. Mass spectrometry analysis

Standard solutions of four tea polyphenols (EGCG, ECG, EGC, EC) were mixed in 0.5 M NaCl solution at a concentration of 0.5 mg/mL. Other polyphenols (chlorogenic acid and ferulic acid) were ddissolved in DIW at a concentration of 1 mg/mL before analysis. For evaluating salt and protein tolerance, standard molecules were mixed with NaCl (0.5 M) and BSA (5 mg/mL) and analyzed by laser desorption/ionization mass spectrometry (LDI MS). Theanine, glucose, sucrose, rhamnose, and arabinose were added to the standard samples at a concentration of 1/10 of the tea polyphenols to eliminate the interferences in real tea.

A series of inorganic matrices (Pt/NiFe-LDH-10/25/50/75/100, Pt NPs, Ni NPs, Fe NPs, and NiFe-LDH, dispersed within DIW at a concentration of 1 mg/mL) were used as matrices for LDI MS. Commercial gold nanoparticles (Au NPs) were directly used as matrices with a concentration of 0.2 g/L. 10 mg of CHCA and DHB were dissolved in 1 mL of TA30 (30:70 (v:v) acetonitrile: TFA 0.1% in water) and used as organic matrices.

During the detection process, typically, 1 μL sample solution was pipetted on the polished target plate and air-dried. Then, 1 μL of the above matrices were added to the sample point separately and dried again, according to the method from existing works [15,30]. Mass spectra were acquired using a Bruker Autoflex Speed mass spectrometer (Germany) equipped with an Nd: YAG laser (2 kHz, 355 nm). All the raw spectra (m/z between 100 and 1000) were produced in positive reflector mode with a fixed laser intensity of 30%.

The standard EC samples at concentrations of 50/60/70/80 μg/mL with 50 μg/mL EGC as internal standards (IS) were analyzed by LDI MS and LC-MS. Calibration curves between the response ratio of EC/EGC and concentration of EC were built by LDI MS and LC-MS analysis respectively. Each sample analysis was repeated three times. The samples were analyzed using Triple Quad™ 4500 MD LC-MS/MS equipped with a Kinetex 2.6 μm C18 100 Å ODS column (50 mm × 2.1 mm i.d.; Phenomenex, Torrance, CA, USA). Elution was carried out at 40 °C, using a 0.03% (v/v) formic acid/water solution as mobile phase A, and methyl alcohol as mobile phase B. A flow rate of 0.4 mL/min was employed and the gradient conditions were as follows: 0 min, 2% B; 0.3 min, 2% B; 1 min, 95% B, 1.6min 95% B, 1.61 min 2% B, and 2 min 2% B. The injection volume was 1 μL. Mass spectrometry data is recorded in ESI positive ion mode. Ion source settings were as follows: temperature 500 °C, ion source gas (1/2) 50 psi, curtain gas 35 psi, collision gas 9 psi, and ion spray voltage 5500 V.

Tea samples were analyzed following a similar protocol. Bio-samples (plasma and serum, ethical approval number: CHEC2021-157) were collected and analyzed [31], with consent obtained for experimentation with human subjects. All the MS findings were directly utilized for molecular identification without prior processing.

2.6. Autoxidation monitoring by LDI MS

0.5 mg/mL glucose and 0.5 mg/mL NaCl were mixed with four polyphenol monomers (EC, EGC, ECG. EGCG, 0.5 mg/mL) standard solutions. Here, glucose was introduced as the internal standard. Briefly, 1 μL of the standard solution was deposited on the target plate for autoxidation. After 0, 1, and 2 h of oxidation, we dropped 1 μL of Pt/NiFe-LDH-50 hybrids on the sample spots and analyzed them by LDI MS.

2.7. Statistical analysis

Principal component analysis (PCA) was performed on Origin 2023. Other univariate analyses were conducted on SPSS software to calculate the p-value by Student's t-test. P-values of <0.05 were regarded as statistically significant.

3. Results

3.1. Preparation and characterization of Pt/NiFe-LDH hybrids

Pt/NiFe-LDHs were synthesized *via* an ultrasound-assisted reduction method, involving ultrasonic peeling and *in-situ* platinum NP deposition. We characterized the NiFe-LDH nanosheets with a stacked-layer structure, by transmission electron microscopy (TEM, Fig. 1A, B-i) and scanning electron microscopy (SEM, Fig. S1A). During the process of platinum reduction, the surface area also increased due to the formation of scattered flake structures by sonication. (Fig. S1B), providing more active sites for further utilization. Pt clusters (marked by yellow ellipses) with a diameter of ~4 nm were observed on nanosheets (Fig. 1A, B-ii), while no Pt NPs were found in locations beyond the NiFe-LDH sheets. The corresponding energy dispersive X-ray spectra were recorded and quantitated a platinum loading ratio of 7.19 wt% after platinum introduction, further confirming the successful assembling of hybrids (Table S1). The obtained hybrids exhibited a uniform distribution of Ni, Fe, and Pt from elemental mapping analysis (Fig. 1C), which agreed with the observations from TEM (Fig. 1A, B-ii). These findings evidenced the stabilizing effect of NiFe LDH crystalline sheets as a support material for the controlled formation and growth of Pt particles at the nanoscale.

Common techniques for loading noble metals encompass chemical impregnation [32], electrodeposition [33], and vapor-phase deposition [34], all of which necessitate harsh experimental conditions such as elevated temperatures, increased pressures, controlled gaseous atmospheres, and specific dispersants. In contrast, we adopted an ultrasound-assisted reduction method, maintaining a homogeneous reaction system while producing small metal particles in a sustainable and green manner [28]. In particular, the interlayer of the LDH sheets acted as a miniaturized nanoreactor, allowing for the confined reduction of Pt^+ cations. The Pt NPs prepared using this method displayed good dispersion, and demonstrated reduced aggregation tendencies.

High-resolution TEM (Fig. 1B) and selected-area electron diffraction pattern (Fig. 1D–E) revealed distinct polycrystalline structures from NiFe-LDH sheets and Pt/NiFe-LDH hybrids. The measured d-spacing in NiFe-LDHs (Fig. 1B–i) matched the typical diffraction planes of (015). Similarly, the measured d-spacing of 0.226 nm and 0.191 nm aligned with the diffraction plane of (111) and (200) of Pt NPs (Fig. 1B–ii). The crystalline structures were further verified using wide-angle X-ray powder diffraction (Fig. 1F) analyses. The diffraction peaks at 39.8°, 46.2°, 67.5°, 81.3°, and 85.7° were assigned to (111), (200), (220), (311), and (222) diffractions for Pt NPs (JCPDS: 87–0647). X-ray photoelectron spectroscopy (XPS) was employed to investigate the surface chemical composition of the Pt/NiFe LDH hybrids. Analysis of the XPS survey revealed signals corresponding to Ni, Fe, O, C, and Pt, indicating the successful incorporation of Pt and NiFe-LDH (Fig. S2A). The Fe^{3+} 2p peaks of the NiFe LDH substrate were observed at 711.75 eV and 723.78 eV in Fig. S2B. Peaks at 855.60 eV and 873.18 eV were identified as the Ni^{2+} 2p peaks, with satellite peaks at 861.08 eV and

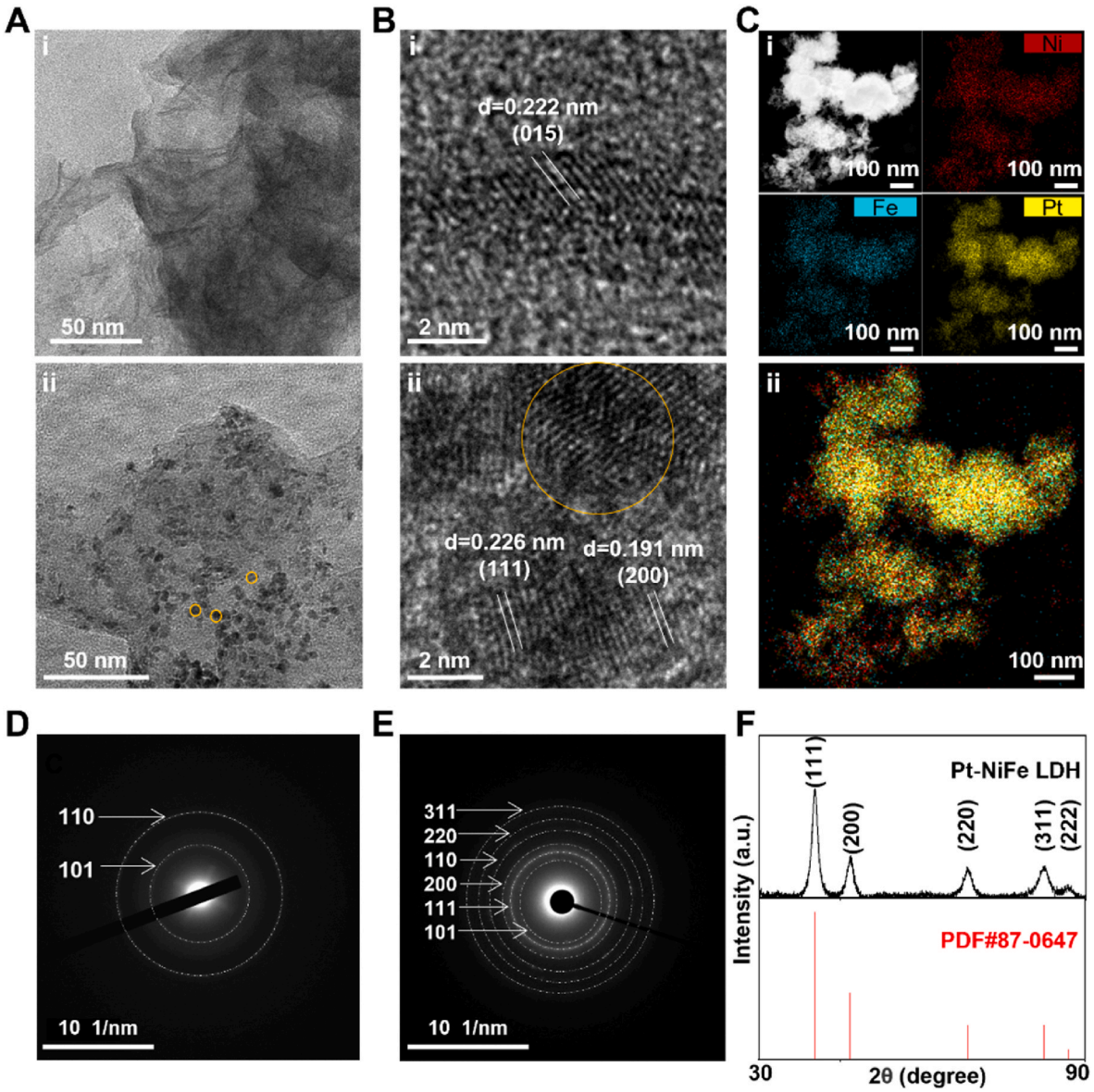

Fig. 1. Preparation and characterization of Pt/NiFe-LDH hybrids. (A, B) Transmission electron microscopy (TEM) images of (i) NiFe-LDH and (ii) Pt/NiFe-LDH at different magnifications. (C) Electron microscopy images, including (i) The high-angle annular dark field-scanning transmission electron microscope (HAADF-STEM) and (i, ii) elemental mapping images of Pt/NiFe-LDH, which indicated Fe (blue), Ni (red), and Pt (yellow). Selected-area electron diffraction (SAED) patterns of (D) NiFe-LDH and (E) Pt/NiFe-LDH. (F) X-ray diffraction (XRD) spectra of Pt/NiFe-LDH and Pt (JCPDS: 87–0647). (For interpretation of the references to color in this figure legend, the reader is referred to the Web version of this article.)

879.78 eV depicted in Fig. S2C. In the core level spectra of Pt, the Pt^0 4f peaks were observed at 71.16 eV and 74.48 eV. Additionally, the Pt $4f_{5/2}$ peak at 75.98 eV and Pt $4f_{7/2}$ peak at 72.58 eV were attributed to a small amount of Pt^{2+}, resulting from incomplete reduction or re-oxidation processes (Fig. S2D). All the results together verified the successful modification of Pt in the hybrids.

Ultrasonic stripping during synthesis increased the reaction surface of nanohybrids, leading to the exposure of more active sites and facilitating the extraction of analytes from complex samples [35]. Moreover, the abundance of hydroxyl groups on the NiFe-LDH surface enhanced the adsorption of hydroxyl-rich molecules (*e.g.*, polyphenols) through binding affinity based on hydrogen bonding [27]. The stable crystal nature of Pt/NiFe-LDH hybrids indicated durability even under laser ablation during LDI MS detection. Acting as a carrier host material for Pt NPs, NiFe-LDH sheets enabled the uniform distribution of Pt, holding promise in suppressing the coffee-ring effect in subsequent LDI MS utilization. Consequently, Pt/NiFe-LDH hybrids, possessing large surface area, preferential analyte adsorption, and stable crystalline structure, are anticipated to contribute to enzymatic and LDI enhancement in the next step.

3.2. Colorimetric detection assisted by hybrids

Colorimetric assay of polyphenols was performed with Pt/NiFe-LDH as catalyst and H_2O_2 as oxidizing agent. These hybrids exhibit peroxidase-like properties, where hybrids catalyze the one-electron oxidation of TMB by H_2O_2 to generate the charge transfer complex of oxidized TMB. The reaction solution yielded a blue-colored product with a maximum absorbance at 652 nm in the presence of H_2O_2, accompanied by the generation of 3,3′,5,5′-tetramethylbenzidine di-imine (TMBDI) catalyzed by the Pt/NiFe-LDH hybrids (Fig. S3). In contrast, no absorbance at 652 nm was observed when only H_2O_2 was added to the TMB solution. Notably, the colorless TMB was oxidized to blue TMBDI only when H_2O_2, TMB, and Pt/NiFe-LDHs were present at the

same time (Fig. 2A–B), suggesting the intrinsic peroxidase-mimic activity of the hybrids for facile colorimetric detection.

According to a standardized method for determining nanozyme activity [29], the catalytic activity of Pt/NiFe-LDH was quantified as 33.472 U/mg (Fig. 2C). Control experiments showed lower activities of 23.148 U/mg and 1.036 U/mg using Pt alone or bare LDH sheets as nanozymes, respectively (Fig. S4). In addition, the Pt/NiFe-LDH nanohybrids yielded a 17-fold enhancement over the typical nanozyme Fe_3O_4, which has a reported activity of 1.958 U/mg and is currently utilized in clinical applications such as biosensing, anti-bacterial, and cancer therapy [29]. Both the components and morphologies decide the catalytic properties of nanozymes [36,37]. In terms of components, both Pt NPs and NiFe-LDH possess intrinsic peroxidase-like activity individually. The hybrids consisting of these two building blocks exhibited higher activity, benefitting from a synergistic effect [38,39]. Regarding morphology, the hybrids provide a greater surface area and more exposed active sites after exfoliation, leading to an augmentation of the interacting force between hydroxyl group-containing analytes (*e.g.*, H_2O_2) and Pt/NiFe-LDH.

Pt/NiFe-LDH hybrids remained active in a wider range of environmental circumstances than natural horseradish peroxidase. The optimized experimental properties for Pt/NiFe-LDH hybrids were determined prior to their application in a clinical colorimetric assay under varying conditions, including reaction temperature, pH, and storage stability, respectively. The catalytic activity of Pt/NiFe-LDH remained stable at 75%–100% within the temperature range of 25–45 °C (Fig. S5A). Various NaAc-HAc buffer solutions with pH values ranging from 3.5 to 5.5 were employed to evaluate the pH resistance of hybrids. As shown in Fig. S5B, the peroxidase-like activity of Pt/NiFe-LDH reached 100% in acidic media (pH of 3.7). Hence, an optimal reaction was achieved at a catalytic temperature of 25 °C and a pH of 3.7, taking into consideration the tradeoff between reaction convenience and detection performance for subsequent analysis. Furthermore, the catalytic performance of Pt/NiFe-LDH hybrids was daily monitored over a 15-day storage period. The relative activities (defined as $SA_{n\text{-}day}/SA_{maximum}$) remained as high as 94% with no significant decrease ($p > 0.05$ and coefficient of variation (CV) of 1.93%) after long-term storage (Fig. 2D).

We further applied the Pt/NiFe-LDH hybrids as the nanozymes for the colorimetric detection of polyphenols. Given the antioxidant property of polyphenols that inhibits TMB oxidation, the intensity of color in the reaction system is directly associated with the concentration of polyphenols present. Employing TMB as the indicator molecule, the ultraviolet–visible (UV–vis) spectra revealed a gradual decrease in absorbance as the polyphenol concentration increased, showcasing the steady-state kinetic equilibrium (Fig. 2E). Specifically, the absorption intensity at 652 nm was linearly proportional ($R^2 = 0.996$) to the concentration of tea polyphenols (Fig. 2F), within a linear range of 10–50 μg/mL ($y = 1.093 - 0.010x$). This linear range aligned with the typical polyphenol concentrations found in real-world samples (*e.g.*, 200–1000 μg/mL in three major categories of tea, including green tea, black tea, and oolong tea). The range was relatively wider over other recently reported polyphenol sensing systems [40], thus holding promise for simple polyphenol quantification.

Notably, the colorimetric platform constructed based on the Pt/NiFe-LDH hybrids featured a fast enzymatic reaction (~1 min) and minimal nanozyme consumption (1 μg), due to excellent peroxidase activity (33.472 U/mg). For comparison, rigorous reaction steps and extended reaction times (approximately hours) were generally required in the standard method (Folin-Ciocalteu colorimetric method). While previous nanozyme-based biosensors have reduced the reaction time for polyphenol quantification to 15–50 min [9,40–42], our platform achieved a minimum 30-fold reduction of time and a 40-100-fold reduction in nanozyme consumption. These results underscore the potential of Pt/NiFe-LDH as a quantitation tool for phenols toward on-site field test applications.

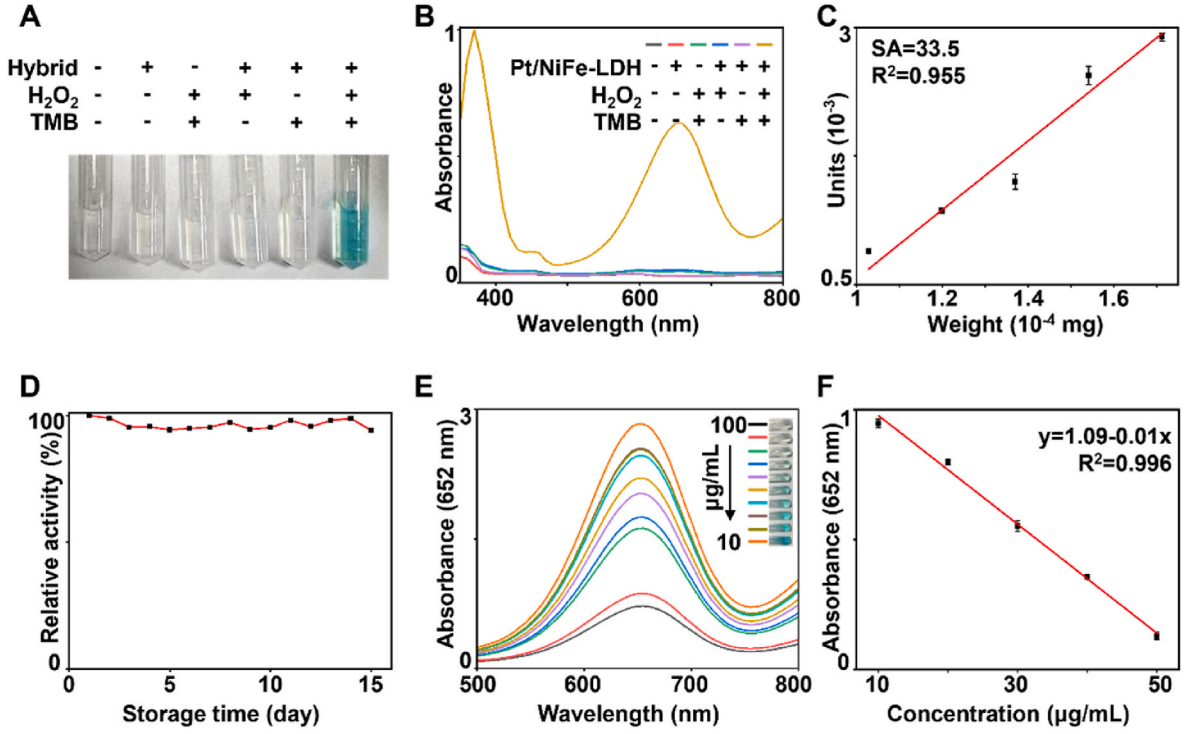

Fig. 2. Colorimetric detection assisted by hybrids. (A) Photographs and (B) ultraviolet–visible (UV–vis) absorption spectra of different reaction systems. (C) The catalytic activity of Pt/NiFe-LDH was acquired according to the nanozyme activity standardization method. (D) The relative activity of Pt/NiFe-LDH during 15 days of storage at room temperature. (E) UV–vis absorption spectra with different concentrations of polyphenols. Inset: color corresponding to the reaction system with different polyphenol concentrations. (F) Linear calibration plot for polyphenol concentration from 10 to 50 μg/mL. (For interpretation of the references to color in this figure legend, the reader is referred to the Web version of this article.)

3.3. LDI MS enhanced by hybrids

We further applied Pt/NiFe-LDH hybrids as matrices for LDI MS use and selected the optimized hybrid for polyphenol detection. We synthesized a series of Pt/NiFe-LDHs by varying the volume of 10 mM chloroplatinic acid (10, 25, 50, 75, and 100 mL, denoted as Pt/NiFe-LDH-10/25/50/75/100). Energy-dispersive X-ray analysis revealed an increased Pt loading ratio for Pt/NiFe-LDH-10/25/50/75/100, with the gradual addition of a precursor (Fig. 3A, Fig. S6A).

We recorded typical sodium-adducted ($[M+Na]^+$) MS spectra of four indicator polyphenols (Fig. 3B), for (−)-epicatechin (EC) at m/z of 313.08, (−)-epigallocatechin (EGC) at m/z of 329.07, (−)-epicatechin gallate (ECG) at m/z of 465.13, and (−)-epigallocatechin gallate (EGCG) at m/z of 481.14. Notably, Pt/NiFe-LDH-50 offered the highest signal intensity for polyphenol standards (Fig. 3C, Fig. S6B), surpassing other hybrids. Excessive platinum loading on the LDH sheets (*e.g.*, Pt/NiFe-LDH-75) diminished the analytical efficiency due to evident clumping and aggregation caused by the surplus of platinum (Fig. S7). On the other hand, inadequate platinum loading (*e.g.*, Pt/NiFe-LDH-25) also impacted the analytical efficiency, as more surface area from the LDH sheets was exposed to analytes and fewer specific platinum NPs were present.

Moreover, the Pt/NiFe-LDH-50 hybrid also demonstrated significantly improved performance (Fig. S8) compared to bare NiFe-LDH and the individual incorporated metals (Pt, Ni, Fe) ($p < 0.05$). As a result, we demonstrated the advantage of using the hybrid for LDI MS over incorporated metals was the high sensitivity. The Pt NPs incorporating NiFe-LDH as substrate promoted an increase in detection efficiency. Photoelectrochemical analyses also provided insight into charge separation at the composite interface (Fig. 3D). Upon the introduction of Pt, we observed the corresponding 5-fold increase in maximum photocurrent response from NiFe-LDH to Pt/NiFe-LDH-50 hybrids, indicating enhanced photoelectric effects through the generation of hot electrons [31]. The elemental synergies and heterogeneous structures in Pt/NiFe-LDH hybrids support their role as a matrix for aiding analyte desorption and ionization processes. Specifically, the larger plasmon damping effect of Pt effectively dissipates the initial excitation energy as heat, thereby enhancing analyte desorption [21]. Additionally, the heterostructure formed at the hybrid interfaces facilitates the mobility of inter-component hot carriers, facilitating the ionization of analytes by reducing the kinetic barrier for interfacial electron transfer [20]. Therefore, we highlighted the advantage of introducing two kinds of different materials into the hybrid composites for enhanced LDI efficiency.

Current LDI MS investigations employed organic acids and other metal NPs as matrices [43]. In our study, we compared the Pt/NiFe-LDH-50 hybrid with organic matrices (α-cyano-4-hydroxycinnamic acid (CHCA) and 2,5-dihydroxybenzoic acid (DHB)) as well as metal matrices (gold NPs) in terms of polyphenol detection performance (Fig. S9). The mass spectrometry data obtained for the four target polyphenols using Pt/NiFe-LDH-50 as the matrix exhibited superior results compared to those obtained using CHCA, DHB, and Au NPs ($p < 0.05$).

We computed the CVs for peak intensities of standard molecules, achieving highly reproducible spectra with CVs of 1.8%–9.6% for intra-batch (Figs. 3F) and 7.8%–11.7% for inter-batch (Fig. S10A) in 5 replicates of 5 samples. We also calculated the CVs in the detection of polyphenol monomers. The reproducibility of polyphenol detection is ensured with CVs of 5.7%–12.0% for intra-batch and 4.7%–10.3% for inter-batch analyses (Fig. S10B). An acceptable CV in the validation of bioanalytical methods should be less than 15% following the guideline of the National Medical Products Administration in China [44]. For comparison, data obtained from organic matrix-enhanced LDI MS (*e.g.*, DHB) demonstrated a maximum CV of 22.3% (Fig. S10C). We attributed the reproducibility of MS data to the homogeneous co-crystallization and uniform distribution of hybrids and analytes.

Subsequently, we investigated the feasibility of using the optimized hybrids as the matrix in LDI MS for real-world samples. In contrast to standards, bio-samples are typically complex mixtures with high concentrations of salts and other macromolecules. We incorporated small

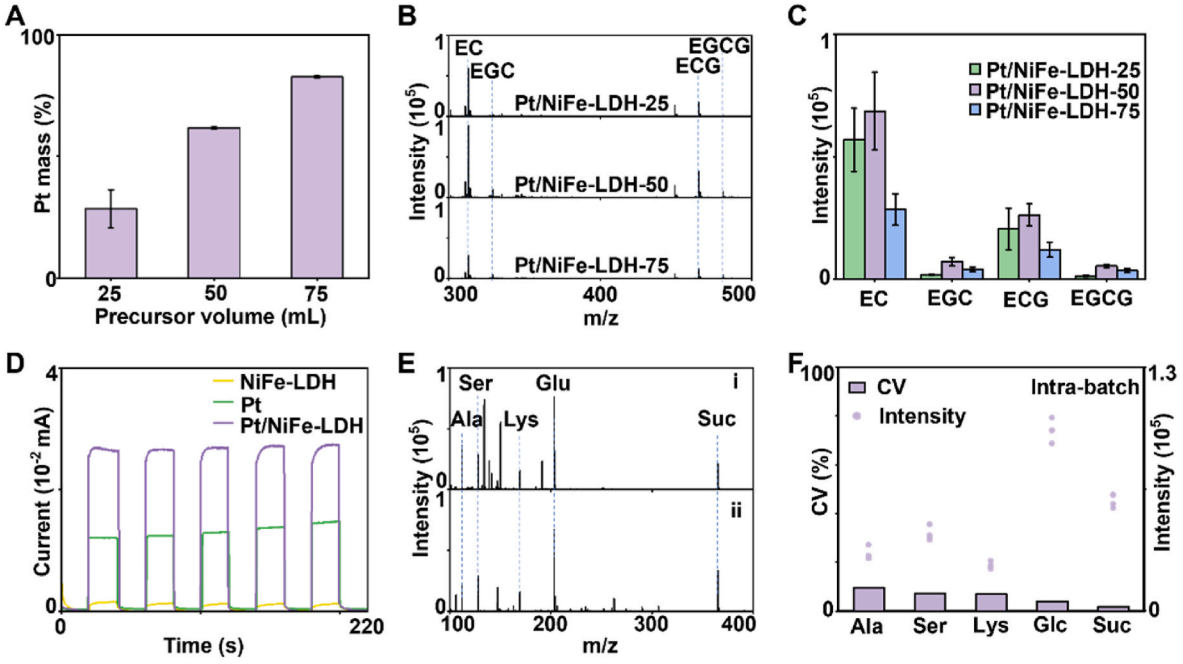

Fig. 3. LDI MS enhanced by hybrids. (A) Elemental composition analysis of Pt/NiFe-LDHs hybrids with different precursor volumes (mL) (B) Typical Pt/NiFe-LDH-enhanced MS spectra of four standard polyphenols. (C) Mean intensities of mass spectra signals of four polyphenols with different matrices including Pt/NiFe-LDH-25/50/75 hybrids. (D) Photocurrent response of NiFe-LDH, Pt, and Pt/NiFe-LDH hybrids. (E) Typical Pt/NiFe-LDH-enhanced LDI MS spectra of (i) five standard metabolites and (ii) MS spectra of the same sample in 0.5 M NaCl and 5 mg/mL bovine serum albumin solution. (F) Intra-batch intensities and coefficients of variation (CVs) of five standard metabolites obtained by Pt/NiFe-LDH-enhanced LDI MS.

molecules with abundant salts (NaCl, 5 mM) and proteins (BSA, 5 mg/mL) [45]. Remarkably, there were no significant differences in signal intensities between the molecular detection with or without salts and proteins (Fig. 3E–ii). We then applied the optimized hybrids to the MS detection of typical hydroxyl-rich small molecules from bio-samples, to further assess the anti-interference ability of the materials. Circulating blood is accessible bio-samples in clinical settings and contains hydroxyl-rich biomarkers for disease diagnosis and prognosis. Using the designer hybrids, we directly detected the Na^+-adducted serine at *m/z* of 148.01 and Na^+-adducted hydroxybutyric acid at *m/z* of 148.99 (Fig. S11), consuming trace serum and plasma samples (down to 0.1 μL only). In real-case tea samples, soluble amino acids (predominantly theanine) and sugars (*e.g.*, glucose, sucrose, rhamnose, and arabinose) are prominent components alongside tea polyphenols [46]. To address potential interferences, we included theanine, glucose, sucrose, rhamnose, and arabinose in the standard polyphenol samples. Analysis of the mass spectra from the mixed samples revealed no significant degradation in the MS signals of tea polyphenols, even in the presence of these interfering substances ($p > 0.05$, Fig. S12). Thus, we validated the Pt/NiFe-LDH as an ideal matrix for the real-case measurements of complex systems.

3.4. Integrated platform for polyphenol detection

Tea polyphenols, generally accounting for 18%–36% of the dry weight of tea leaves, predominantly encompass four catechins, including EC, ECG, EGC, and EGCG. The bioavailability of tea polyphenols has currently attracted great interest in disease treatments owing to their antioxidant, anti-inflammatory, and anticarcinogenic properties. As a proof-of-concept study, we constructed a two-step platform for polyphenol detection, integrating the polyphenol quantitation by colorimetric method and qualification by LDI MS, both based on Pt/NiFe-LDH hybrids (Fig. 4A). In particular, the hybrid was applied for LDI MS to identify polyphenols and their autoxidation products only. Furthermore, the hybrids served as the matrix to enhance desorption and ionization efficacy in LDI MS, distinct from their role as nanozymes in the colorimetric quantitation assay.

In the first step, we detected total tea polyphenols from 9 tea samples by Pt/NiFe-LDH-enhanced colorimetric platform (Fig. 4B). The averaged concentrations of tea polyphenols were quantified as 661, 662, and 465 μg/mL for green tea, oolong tea, and black tea, respectively (Fig. 4B). Tea classification is based on the level of fermentation, impacting the varying abundance of polyphenols across different tea types. Green and oolong teas, with lighter fermentation processes, exhibited higher polyphenol content compared to black tea. Our quantification findings aligned with the expected levels of tea polyphenols as

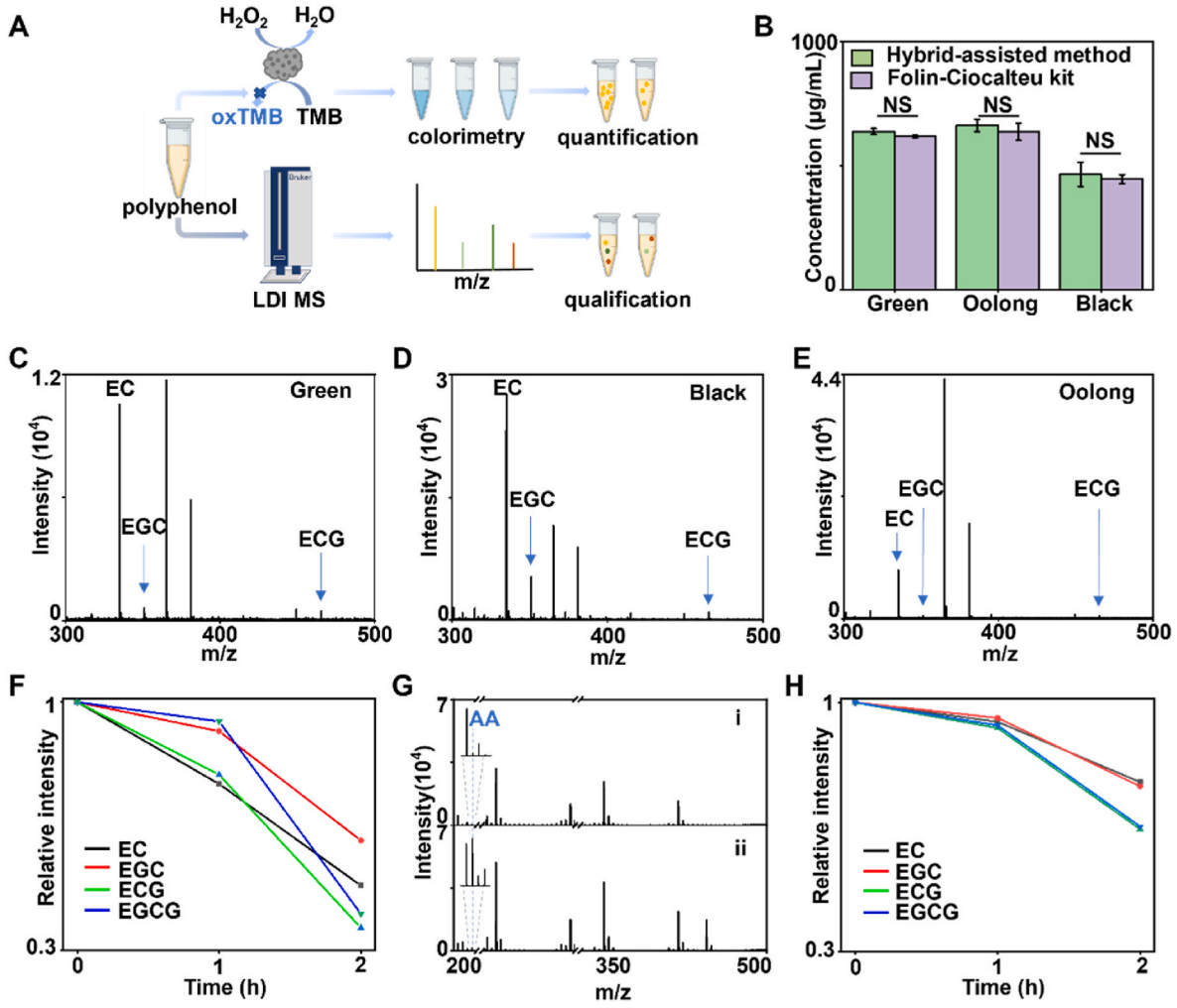

Fig. 4. Integrated platform for polyphenol detection. (A) Schematic diagram of the platform. (B) Comparison of quantitative results obtained by Pt/NiFe assisted colorimetric method and Folin-Ciocalteu colorimetric method. (C–E) Typical MS spectra of tea polyphenols from green tea, black tea, and Oolong tea. (F) Relative intensity changes of four catechins stored at 25 °C. (G) MS spectra of four catechins with (ii) and without (i) ascorbic acid (AA) added. (H) Relative intensity changes of four catechins with AA addition at 25 °C. (For interpretation of the references to color in this figure legend, the reader is referred to the Web version of this article.)

indicated in these three tea varieties as well as previous literature [47]. The quantitation results demonstrated consistency with a commercial assay kit (Folin-Ciocalteu colorimetric method), yielding a coefficient of determination (R^2) of 0.949 (Fig. S13A). Notably, the polyphenol quantification by Pt/NiFe-LDH-enhanced colorimetric method resulted in an average recovery of 100.18% ± 1.16% with a CV of 1.16%, which was comparable to the commercial kit that yielded an average recovery of 99.72% with a CV of 4.36% (Fig. S13B).

In the second step, we performed LDI MS on tea samples by using Pt/NiFe-LDH as matrices and distinguished four tea polyphenols according to their accurate molecular weights. We recorded the typical mass spectra of tea samples and observed clear characteristic MS peaks of catechins, at *m/z* 335.10 $[M+2Na–H]^+$ for EC, *m/z* 351.06 $[M+2Na–H]^+$ for EGC, and *m/z* 465.00 $[M+Na]^+$ for ECG. In addition to the phenolic acids that catechins are classified under, flavonoids and stilbenoids represent other major classes of polyphenols. For our study on the generalizability of polyphenol identification using LDI MS, we selected chlorogenic acid and ferulic acid as indicator analytes. This analysis yielded clear sodium-adducted ($[M+Na]^+$) mass spectra, for chlorogenic acid at *m/z* of 377.07 and ferulic acid at *m/z* 217.06 (Fig. S14). Particularly, distinct peak intensities for catechins were observed in three types of tea samples (green tea, oolong tea, and black tea, Fig. 4C–E), suggesting the potential for tea quality identification and control based on their unique catechin fingerprints. Given the variations in the type and abundance of compounds in different types of tea, we applied principal component analysis to assess all extracted fingerprints from the mass spectra of diverse tea samples. The scatter plot demonstrated that the data derived from mass spectra effectively distinguished between tea types (Fig. S14C).

We further monitored the redox reaction of catechins by Pt/NiFe-LDH-enhanced LDI MS for a consecutive 2-h period (Fig. 4F). Specifically, in the LDI MS analysis, the autoxidation products of catechins were analyzed, including δ-type dehydrodicatechins, dihydro-indenecarboxylic acid, theasinensin, *etc*. In a typical reaction, catechins undergo auto-oxidation due to their highly reactive attributes, independent of any enzymes. Accordingly, we observed a decrease in the relative signal intensities ($intensity^{+}_{[M+Na]}/intensity^{+}_{[Glu\ +\ Na]}$) of the sodium salt of four catechins respectively. Taking EC as an example, we recorded increasing relative signal intensity of the primary auto-oxidative products (*e.g.*, δ-type dehydrodicatechins, Fig. S15). In particular, the signal intensities of EGCG and EGC displayed a more rapid decline as compared to EC and ECG, suggesting their active nature. The different degradation efficiency of catechins correlates with their antioxidant properties, as the oxidation rate varies based on the number of hydroxyl groups present in different catechins [48]. We also investigated the antioxygen functions of ascorbic acid on catechins. Upon the introduction of ascorbic acid, we validated the presence of ascorbic acid, as indicated by the Na^+ adducted signal at *m/z* 199.01 as compared to the original system (Fig. 4G). Following a 2-h reaction, the addition of ascorbic acid resulted in a maximum 2-fold decrease in the degradation rate of all catechins (Fig. 4H).

The LDI MS method is featured by fast analysis speed for qualification studies but lacks sufficient accuracy for quantitation applications. To address this flaw, we replaced conventional organic matrices with inorganic hybrids, facilitating the formation of uniform co-crystals between analytes and the matrix. This approach eliminates the manual search for the optimal analysis spot, enhancing the accuracy of quantitative analyses. As a result, the experimental ratio between EC and EGC (internal standard) was linearly proportional ($R^2 = 0.999$, $y = 0.014x-0.237$) to the concentration of analyte (EC) with an average recovery of 98.75% and a relative standard deviation (RSD) of 1.8% (Fig. S16A). Currently, the LC-MS method has already adopted a widely recognized analytical technique. The detection performance acquired from the developed LDI MS was comparable to that from LC-MS, which yielded an average recovery of 100.68% with an RSD of 1.2% (Fig. S16B). In addition to quantitation accuracy, LDI MS offered advantages in terms of sample preparation and detection time (Table S2), making it more suitable for the swift detection and monitoring of polyphenol monomers with chemical activities.

To confirm the feasibility of large-scale applications, we calculated the yield rate and consumption of the Pt/NiFe-LDH hybrids on three replicates. Our synthesis strategy exhibited a satisfactory yield of 63.56% per pass of chloroplatinic acid hexahydrate (50 mL, 10 mM), defined as the mole ratio between final products and theoretical products. An average of about 100 mg of the final product was produced from three batches, enough for 100,000 tests (1 μg/test), indicating its potential for large-scale applications.

This work offered a reference method for the rapid quantitation of polyphenols and accurate quantitation of polyphenol fingerprints. The optimized Pt/NiFe-LDH hybrids, designed with peroxidase activity, heterogeneous structure, and preferential affinity toward polyphenols, are pivotal in the development of this integrated platform. Notably, the platform featured a shortened detection time (*e.g.*, ~2 min per sample), making it suitable for on-site field applications. Moreover, the hybrid-enhanced LDI MS consumed 250 times fewer samples (200 nL at most) within a shortened duration (~seconds), enabling the direct monitoring of the oxidation-reduction reaction of phenolic substances.

4. Conclusion

To further validate this approach, collecting more biofluid samples from individuals who have consumed polyphenols is necessary. In the context of drug delivery, the collection of biofluid samples from animal models is also crucial for investigating the release and metabolism of catechin. This analysis will play a key role in assessing the efficacy of monitoring polyphenol bioavailability through the integrated platform utilizing Pt/NiFe-LDH hybrids, particularly in scenarios related to catechin pharmacokinetics in clinical and research environments.

In summary, we developed an integrated platform that supports the quantification and qualification of polyphenols based on Pt/NiFe-LDH hybrids. The platform facilitated the fast and easy quantitation of total polyphenols, accurate identification of polyphenol monomers, and monitoring the decomposition of unstable polyphenols. This strategy could be expanded to develop assays for various polyphenols aimed at bioavailability evaluation.

CRediT authorship contribution statement

Chunmeng Ding: Writing – original draft, Validation, Methodology, Data curation. **Yuexing Zhu:** Writing – original draft, Resources, Investigation. **Zhiyuan Huo:** Validation. **Shouzhi Yang:** Writing – review & editing, Conceptualization. **Yan Zhou:** Methodology. **Ayizekeranmu Yiming:** Methodology. **Wei Chen:** Writing – review & editing. **Shanrong Liu:** Writing – review & editing, Resources. **Kun Qian:** Writing – review & editing, Supervision, Project administration, Methodology, Funding acquisition, Conceptualization. **Lin Huang:** Writing – review & editing, Visualization, Supervision, Project administration, Methodology, Funding acquisition, Conceptualization.

Declaration of competing interest

The authors declare the following financial interests/personal relationships which may be considered as potential competing interests: Kun Qian and Lin Huang has patent pending to Shanghai Jiao Tong University. If there are other authors, they declare that they have no known competing financial interests or personal relationships that could have appeared to influence the work reported in this paper.

Data availability

Data will be made available on request.

Acknowledge

The authors thank the financial support from the National Natural Science Funds (Grant No. 82372148), National Key R&D Program of China (Nos. 2021YFF0703500, 2022YFE0103500), Medical-Engineering Joint Funds of Shanghai Jiao Tong University (Nos. YG2021ZD09, YG2022QN107, YG2023ZD08), and Shanghai Institutions of Higher Learning (No. 2021-01-07-00-02-E00083). This work was also sponsored by the Innovative Research Team of High-Level Local Universities in Shanghai (SHSMU-ZDCX20210700), Innovation Group Project of Shanghai Municipal Health Commission (2019CXJQ03), Innovation Research Plan by the Shanghai Municipal Education Commission (ZXWF082101), National Research Center for Translational Medicine Shanghai (Nos. TMSK-2021-124, NRCTM(SH)-2021-06), and Medical-Engineering Joint Funds of University of Shanghai for Science and Technology (2023GD-XK01Z).

Appendix A. Supplementary data

Supplementary data to this article can be found online at https://doi.org/10.1016/j.mtbio.2024.101047.

References

[1] Y. Li, D. He, B. Li, M.N. Lund, Y. Xing, Y. Wang, F. Li, X. Cao, Y. Liu, X. Chen, J. Yu, J. Zhu, M. Zhang, Q. Wang, Y. Zhang, B. Li, J. Wang, X. Xing, L. Li, Engineering polyphenols with biological functions via polyphenol-protein interactions as additives for functional foods, Trends Food Sci. Technol. 110 (2021) 470–482, https://doi.org/10.1016/j.tifs.2021.02.009.

[2] R. Gan, H. Li, Z. Sui, H. Corke, Absorption, metabolism, anti-cancer effect and molecular targets of epigallocatechin gallate (EGCG): an updated review, Crit. Rev. Food Sci. Nutr. 58 (2017) 924–941, https://doi.org/10.1080/10408398.2016.1231168.

[3] K. Hayat, H. Iqbal, U. Malik, U. Bilal, S. Mushtaq, Tea and its consumption: benefits and risks, Crit. Rev. Food Sci. Nutr. 55 (2015) 939–954, https://doi.org/10.1080/10408398.2012.678949.

[4] M. Oroian, I. Escriche, Antioxidants: characterization, natural sources, extraction and analysis, Food Res. Int. 74 (2015) 10–36, https://doi.org/10.1016/j.foodres.2015.04.018.

[5] A. Yaskolka Meir, E. Rinott, G. Tsaban, H. Zelicha, A. Kaplan, P. Rosen, I. Shelef, I. Youngster, A. Shalev, M. Blüher, U. Ceglarek, M. Stumvoll, K. Tuohy, C. Diotallevi, U. Vrhovsek, F. Hu, M. Stampfer, I. Shai, Effect of green-Mediterranean diet on intrahepatic fat: the DIRECT PLUS randomised controlled trial, Gut 70 (2021) 2085–2095, https://doi.org/10.1136/gutjnl-2020-323106.

[6] Y. Guo, Q. Sun, F.G. Wu, Y. Dai, X. Chen, Polyphenol-containing nanoparticles: synthesis, properties, and therapeutic delivery, Adv. Mater. 33 (2021) 2007356, https://doi.org/10.1002/adma.202007356.

[7] H. Teng, L. Chen, Polyphenols and bioavailability: an update, Crit. Rev. Food Sci. Nutr. 59 (2019) 2040–2051, https://doi.org/10.1080/10408398.2018.1437023.

[8] D. Granato, F. Shahidi, R. Wrolstad, P. Kilmartin, L.D. Melton, F.J. Hidalgo, K. Miyashita, J.v. Camp, C. Alasalvar, A.B. Ismail, S. Elmore, G.G. Birch, D. Charalampopoulos, S.B. Astley, R. Pegg, P. Zhou, P. Finglas, Antioxidant activity, total phenolics and flavonoids contents: should we ban in vitro screening methods? Food Chem. 264 (2018) 471–475, https://doi.org/10.1016/j.foodchem.2018.04.012.

[9] Y. Guan, Y. Lu, J. Zhao, W. Huang, Y. Liu, Cobalt-based zeolitic imidazole framework incorporated with well-dispersed bimetallic nanoparticles/ions as a multifunctional nanozyme for the degradation of environmental pollutants and discrimination of various phenolic substances, Chem. Eng. J. 465 (2023) 142703, https://doi.org/10.1016/j.cej.2023.142703.

[10] J. Wang, R. Huang, W. Qi, R. Su, Z. He, Preparation of amorphous MOF based biomimetic nanozyme with high laccase- and catecholase-like activity for the degradation and detection of phenolic compounds, Chem. Eng. J. 434 (2022) 134677, https://doi.org/10.1016/j.cej.2022.134677.

[11] S. Liu, J. Xu, Y. Xing, T. Yan, S. Yu, H. Sun, J. Liu, Nanozymes as efficient tools for catalytic therapeutics, View 3 (2021) 20200147, https://doi.org/10.1002/viw.20200147.

[12] M. Umehara, K. Yanae, H. Maruki-Uchida, M. Sai, Investigation of epigallocatechin-3-O-caffeoate and epigallocatechin-3-O-p-coumaroate in tea leaves by LC/MS-MS analysis, Food Res. Int. 102 (2017) 77–83, https://doi.org/10.1016/j.foodres.2017.09.086.

[13] W. Chen, H. Yu, Y. Hao, W. Liu, R. Wang, Y. Huang, J. Wu, L. Feng, Y. Guan, L. Huang, K. Qian, Comprehensive metabolic fingerprints characterize neuromyelitis optica spectrum disorder by nanoparticle-enhanced laser desorption/ionization mass spectrometry, ACS Nano 17 (2023) 19779–19792, https://doi.org/10.1021/acsnano.3c03765.

[14] L. Bai, F. Bu, X. Li, S. Zhang, L. Min, Mass spectrometry-based extracellular vesicle micromolecule detection in cancer biomarker discovery: an overview of metabolomics and lipidomics, View 4 (2023) 20220086, https://doi.org/10.1002/viw.20220086.

[15] Y. Zhou, X. Li, Y. Zhao, S. Yang, L. Huang, Plasmonic alloys for quantitative determination and reaction monitoring of biothiols, J. Mater. Chem. B 11 (2023) 8639–8648, https://doi.org/10.1039/d3tb01076g.

[16] Z. Xu, Y. Huang, C. Hu, L. Du, Y.-A. Du, Y. Zhang, J. Qin, W. Liu, R. Wang, S. Yang, J. Wu, J. Cao, J. Zhang, G.-P. Chen, H. Lv, P. Zhao, W. He, X. Wang, M. Xu, P. Wang, C. Hong, L.-T. Yang, J. Xu, J. Chen, Q. Wei, R. Zhang, L. Yuan, K. Qian, X. Cheng, Efficient plasma metabolic fingerprinting as a novel tool for diagnosis and prognosis of gastric cancer: a large-scale, multicentre study, Gut 72 (2023) 2051–2067, https://doi.org/10.1136/gutjnl-2023-330045.

[17] L. Huang, Y. Zhou, Y. Zhu, H. Su, S. Yang, L. Feng, L. Zhao, S. Liu, K. Qian, Dual-modal nanoplatform integrated with smartphone for hierarchical diabetic detection, Biosens. Bioelectron. 210 (2022) 114254, https://doi.org/10.1016/j.bios.2022.114254.

[18] G.V. Hartland, L.V. Besteiro, P. Johns, A.O. Govorov, What's so hot about electrons in metal nanoparticles? ACS Energy Lett. 2 (2017) 1641–1653, https://doi.org/10.1021/acsenergylett.7b00333.

[19] L. Xu, Y. Xie, J. Lin, A. Wu, T. Jiang, Advancements in SERS-based biological detection and its application and perspectives in pancreatic cancer. View, 20230070. https://doi.org/10.1002/viw.20230070, 2023.

[20] H. Zheng, H. Li, W. Song, Z. Zhao, G. Henkelman, Calculations of hydrogen associative desorption on mono- and bimetallic catalysts, J. Phys. Chem. C 125 (2021) 12028–12037, https://doi.org/10.1021/acs.jpcc.1c03466.

[21] Y. Yang, X. Long, F. Zhang, H. Yan, G. Li, M. Luoshan, C. Huang, L. Zhou, Highly uniform AuPt bimetallic nanoplates and nanorings with tunable optical properties and enhanced photothermal conversion performance in NIR-II window, Plasmonics 18 (2023) 889–897, https://doi.org/10.1007/s11468-023-01799-9.

[22] L. Li, Z. Qiu, Y. Qi, D. Zhao, I. Ali, C. Sun, L. Xu, Z. Zheng, C. Ma, AuNPs/NiFe-LDHs-assisted laser desorption/ionization mass spectrometry for efficient analysis of metronidazole and its metabolites in water samples, J. Hazard Mater. 423 (2022) 126893, https://doi.org/10.1016/j.jhazmat.2021.126893.

[23] S. Du, Z. Ren, X. Wang, J. Wu, H. Meng, H. Fu, Controlled atmosphere corrosion engineering toward inhomogeneous NiFe-LDH for energetic oxygen evolution, ACS Nano 16 (2022) 7794–7803, https://doi.org/10.1021/acsnano.2c00332.

[24] J.M. Huo, Z.L. Ma, Y. Wang, Y.J. Cao, Y.C. Jiang, S.N. Li, Y. Chen, M.C. Hu, Q. G. Zhai, Monodispersed Pt sites supported on NiFe-LDH from Synchronous Anchoring and reduction for high efficiency Overall water splitting, Small 19 (2023), https://doi.org/10.1002/smll.202207044.

[25] Y. Wang, C. Jiang, Y. Le, B. Cheng, J. Yu, Hierarchical honeycomb-like Pt/NiFe-LDH/rGO nanocomposite with excellent formaldehyde decomposition activity, Chem. Eng. J. 365 (2019) 378–388, https://doi.org/10.1016/j.cej.2019.01.187.

[26] Y. Pei, W. Cheng, R. Liu, H. Di, Y. Jiang, C. Zheng, Z. Jiang, Synergistic effect and mechanism of nZVI/LDH composites adsorption coupled reduction of nitrate in micro-polluted water, J. Hazard Mater. 464 (2024) 133023, https://doi.org/10.1016/j.jhazmat.2023.133023.

[27] Q. Xu, R. Tian, C. Lu, Mass spectrometry imaging of low-molecular-weight phenols liberated from plastics, Anal. Chem. 93 (2021) 13703–13710, https://doi.org/10.1021/acs.analchem.1c03397.

[28] S. Anantharaj, K. Karthick, M. Venkatesh, T.V.S.V. Simha, A.S. Salunke, L. Ma, H. Liang, S. Kundu, Enhancing electrocatalytic total water splitting at few layer Pt-NiFe layered double hydroxide interfaces, Nano Energy 39 (2017) 30–43, https://doi.org/10.1016/j.nanoen.2017.06.027.

[29] B. Jiang, D. Duan, L. Gao, M. Zhou, K. Fan, Y. Tang, J. Xi, Y. Bi, Z. Tong, G.F. Gao, N. Xie, A. Tang, G. Nie, M. Liang, X. Yan, Standardized assays for determining the catalytic activity and kinetics of peroxidase-like nanozymes, Nat. Protoc. 13 (2018) 1506–1520, https://doi.org/10.1038/s41596-018-0001-1.

[30] J. Cao, Q.J. Yao, J. Wu, X. Chen, L. Huang, W. Liu, K. Qian, J.-J. Wan, B.O. Zhou, Deciphering the metabolic heterogeneity of hematopoietic stem cells with single-cell resolution, Cell Metabol. 36 (2024) 209–221, https://doi.org/10.1016/j.cmet.2023.12.005.

[31] H. Su, X. Li, L. Huang, J. Cao, M. Zhang, V. Vedarethinam, W. Di, Z. Hu, K. Qian, Plasmonic alloys reveal a distinct metabolic phenotype of early gastric cancer, Adv. Mater. 33 (2021) 2007978, https://doi.org/10.1002/adma.202007978.

[32] T. Cai, P. Zhang, X. Shen, E. Huang, X. Shen, J. Shi, Z. Wang, Q. Sun, Synthesis of Pt-Loaded NiFe-LDH nanosheets on wood veneer for efficient gaseous formaldehyde degradation, ACS Appl. Mater. Interfaces 12 (2020) 37147–37154, https://doi.org/10.1021/acsami.0c09016.

[33] Y. Feng, R. Ma, M. Wang, J. Wang, T. Sun, L. Hu, J. Zhu, Y. Tang, J. Wang, Crystallinity effect of NiFe LDH on the growth of Pt nanoparticles and hydrogen evolution performance, J. Phys. Chem. Lett. 12 (2021) 7221–7228, https://doi.org/10.1021/acs.jpclett.1c02095.

[34] H. Li, Y. Li, A. Aljarb, Y. Shi, L. Li, Epitaxial growth of two-dimensional layered transition-metal dichalcogenides: growth mechanism, controllability, and scalability, Chem. Rev. 118 (2017) 6134–6150, https://doi.org/10.1021/acs.chemrev.7b00212.

[35] X. Li, X. Hao, Z. Wang, A. Abudula, G. Guan, In-situ intercalation of NiFe LDH materials: an efficient approach to improve electrocatalytic activity and stability for water splitting, J. Power Sources 347 (2017) 193–200, https://doi.org/10.1016/j.jpowsour.2017.02.062.

[36] W. Yang, X. Yang, L. Zhu, H. Chu, X. Li, W. Xu, Nanozymes: activity origin, catalytic mechanism, and biological application, Coord. Chem. Rev. 448 (2021) 214170, https://doi.org/10.1016/j.ccr.2021.214170.

[37] Z. Huang, X. Sun, P. Wang, H. Wan, Emerging single-atom catalysts in electrochemical biosensing, View 4 (2023) 20220058, https://doi.org/10.1002/viw.20220058.

[38] S.W. Jang, S. Dutta, A. Kumar, Y.-R. Hong, H. Kang, S. Lee, S. Ryu, W. Choi, I. S. Lee, Holey Pt Nanosheets on NiFe-hydroxide laminates: synergistically enhanced electrocatalytic 2D interface toward hydrogen evolution reaction, ACS Nano 14 (2020) 10578–10588, https://doi.org/10.1021/acsnano.0c04628.
[39] R. Yang, Y. Gao, Z. Ouyang, X. Shi, M. Shen, Gold nanostar-based complexes applied for cancer theranostics, View 3 (2022) 20200171, https://doi.org/10.1002/viw.20200171.
[40] J. Zhang, Y. Li, X. Gong, Y. Wang, W. Fu, Colorimetric detection of total antioxidants in green tea with oxidase-mimetic CoOOH nanorings, Colloids Surf., B 218 (2022) 112711, https://doi.org/10.1016/j.colsurfb.2022.112711.
[41] S. Wu, D. Guo, X. Xu, J. Pan, X. Niu, Colorimetric quantification and discrimination of phenolic pollutants based on peroxidase-like Fe_3O_4 nanoparticles, Sensor. Actuator. B Chem. 303 (2020) 127225, https://doi.org/10.1016/j.snb.2019.127225.
[42] Q. Li, D. Yang, Q. Yin, W. Li, Y. Yang, Graphitic carbon nitride nanosheets decorated with Cu-doped carbon dots for the detection and degradation of phenolic pollutants, ACS Appl. Nano Mater. 5 (2022) 1925–1934, https://doi.org/10.1021/acsanm.1c03551.
[43] A.S. Kulkarni, L. Huang, K. Qian, Material-assisted mass spectrometric analysis of low molecular weight compounds for biomedical applications, J. Mater. Chem. B 9 (2021) 3622–3639, https://doi.org/10.1039/d1tb00289a.
[44] Bioanalytical method validation and sample analysis, National Medical Products Administration in China. https://www.cde.org.cn/ichWeb/guideIch/downloadAtt/2/dc63aea35f11de58af52831be02a9c8b, (assessed 5 January 2023).
[45] X. Liu, N. Song, D. Qian, S. Gu, J. Pu, L. Huang, J. Liu, K. Qian, Porous inorganic materials for bioanalysis and diagnostic applications, ACS Biomater. Sci. Eng. 8 (2021) 4092–4109, https://doi.org/10.1021/acsbiomaterials.1c00733.
[46] U.H. Engelhardt, Chemistry of Tea, Comprehensive Natural Products II, Elsevier. Ltd., Amsterdam, 2010.
[47] N. Sanlier, B.B. Gokcen, M. Altuğ, Tea consumption and disease correlations, TRENDS FOOD SCI TECH 78 (2018) 95–106, https://doi.org/10.1016/j.tifs.2018.05.026.
[48] Z. Yin, T. Zheng, C.-T. Ho, Q. Huang, Q. Wu, M. Zhang, Improving the stability and bioavailability of tea polyphenols by encapsulations: a review, Food Sci. Hum. Wellness 11 (2022) 537–556, https://doi.org/10.1016/j.fshw.2021.12.011.